OPTIMAL ELECTRODYNAMIC TETHER PHASING MANEUVERS

Matthew S. Bitzer and Christopher D. Hall

Virginia Tech, Blacksburg, VA, 24060

August 15, 2007

Abstract

We study the minimum-time orbit phasing maneuver problem for a constant-current electrodynamic tether (EDT). The EDT is assumed to be a point mass and the electromagnetic forces acting on the tether are always perpendicular to the local magnetic field. After deriving and non-dimensionalizing the equations of motion, the only input parameters become current and the phase angle. Solution examples, including initial Lagrange costates, time of flight, thrust plots, and thrust angle profiles, are given for a wide range of current magnitudes and phase angles. The two-dimensional cases presented use a non-tilted magnetic dipole model, and the solutions are compared to existing literature. We are able to compare similar trajectories for a constant thrust phasing maneuver and we find that the time of flight is longer for the constant thrust case with similar initial thrust values and phase angles. Full three-dimensional solutions, which use a tilted magnetic dipole model, are also analyzed for orbits with small inclinations.

Nomenclature

a	Reference orbit radius	$R_\circ$	Radius of the earth
$\mathbf{B}$	Magnetic Field Vector	$\hat{\mathbf{R}}$	Position unit vector
$\mathbf{d}$	Derivative of State Vector	T	Dimensionless thrust
$\mathbf{F}$	Force vector	T_0	Dimensionless thrust at original orbit radius
$F : \hat{\mathbf{o}}_1, \hat{\mathbf{o}}_2, \hat{\mathbf{o}}_3$	Magnetic Field Frame	TU	Time Unit
H	Hamiltonian	v_x, v_y, v_z	Velocity components
H_0	Total dipole strength	x, y, z	Position components
i	Current	β	Thrust Coefficient
$\mathbf{L}$	Tether direction vector	ϕ	Phase angle
m	Mass	$\lambda_{()}$	Lagrange costate
$\hat{\mathbf{m}}$	Dipole direction unit vector	μ	Gravitational parameter for attractive body
n	Reference mean orbit velocity	ψ	Thrust control angle
$N : \hat{\mathbf{n}}_1, \hat{\mathbf{n}}_2, \hat{\mathbf{n}}_3$	Inertial Coordinate Frame	ρ	Lagrange costate ratio
r	Orbit radius	$\dot{()}$	Inertial time derivative

1   Introduction

Using an electrodynamic tether (EDT) as a means of propulsion is a relatively new concept that has not been fully developed. There is much in the literature concerning the trajectories of EDTs,[1–5] and Williams gives some solutions for optimal control of an EDT.[1] However, the equations of motion developed in the literature are based on dimensional parameters, making the results specific to the cases presented. Also, in many studies involving EDTs,[1,4] the magnetic field model is a non-tilted dipole. There are no other

known studies that use a tilted dipole model in an optimal control problem. Some other assumptions include restricting the EDT orbit to the equatorial plane and aligning the EDT with the nadir, or radial, direction. This is an unrealistic assumption for any practical application.[2–5] All of these assumptions do not produce enough information create a usable control model.

2 Model

This section will describe the basic physics behind the EDT and how the physics leads to the development of the coordinate system used in analysis.

2.1 Physics

The EDT creates thrust by using a Lorentz force, which is defined by the following equation,

$$\mathbf{F} = i\mathbf{L} \times \mathbf{B} \tag{1}$$

where $\mathbf{F}$ is the force, i a scalar current value, $\mathbf{L}$ is the tether vector, and $\mathbf{B}$ is the magnetic field vector. As the conductive tether moves through the earth's magnetic field, the field induces a current through the wire to counter the change in magnetic flux passing through the tether. The induced current creates a Lorentz force in the opposite direction of flight, slowing the EDT and reducing its orbit altitude.[6] Essentially the tether is converting orbit energy to electrical power in the tether. If the EDT supplies its own current, it can create a force in the direction of travel to accelerate the EDT and raise its altitude. Because the tether is not a circuit, it cannot complete the circuit on its own. It needs free electrons from the earth's ionosphere. Devices on each end of the tether exchange electrons from the ambient plasma. An illustration of this process is seen in Figure 1. Because the EDT must operate in the ionosphere, the orbit altitude must be below about 2000 km. However, this range includes all current manned missions and all other space applications requiring a low earth orbit.
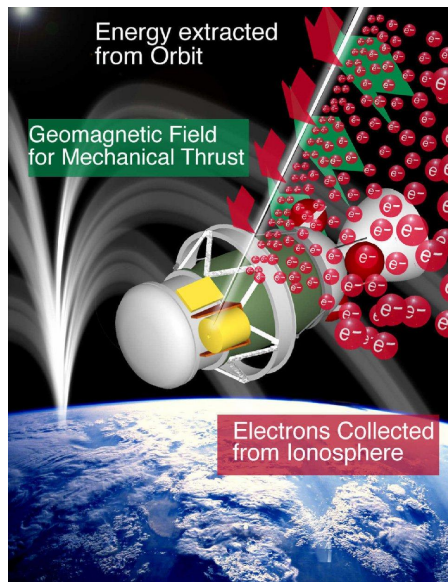

Figure 1: Physics Behind EDT Operation[7]

2.2 Coordinate System and Magnetic Field Model

This optimization problem uses two coordinate frames: an Earth-centered inertial frame, or ECI frame, and a magnetic field frame, F. The ECI frame is defined as $N : \hat{\mathbf{n}}_1, \hat{\mathbf{n}}_2, \hat{\mathbf{n}}_3$, where $\hat{\mathbf{n}}_1$ is in the Vernal Equinox

direction, $\hat{\mathbf{n}}_3$ is parallel to the earth's axis of rotation, and $\hat{\mathbf{n}}_2$ is the cross product of $\hat{\mathbf{n}}_3$ and $\hat{\mathbf{n}}_1$. The magnetic field frame, $F : \hat{\mathbf{o}}_1, \hat{\mathbf{o}}_2, \hat{\mathbf{o}}_3$ is described below.

The $\mathbf{B}$ vector points in the direction of the earth's magnetic field at a given point in space, as shown in Figure 2. The magnetic field used in this problem is based on the tilted dipole model.[8] In vector form, the direction and magnitude of the magnetic field are given by

$$\mathbf{B}(\mathbf{R}) = \frac{R_\circ H_0}{R^3} \left(3 \left(\hat{\mathbf{m}} \bullet \hat{\mathbf{R}} \right) \hat{\mathbf{R}} - \hat{\mathbf{m}} \right) \tag{2}$$

where $R_\circ$ is the radius of the earth, H_0 is the total dipole strength, $\hat{\mathbf{m}}$ is the dipole direction, and $\hat{\mathbf{R}}$ is the normalized position vector. The International Association of Geomagnetism and Aeronomy defines the dipole direction and total magnetic field strength in the International Geomagnetic Reference Field report.[8] The unit vector of $\mathbf{B}$ defines $\hat{\mathbf{o}}_3$.
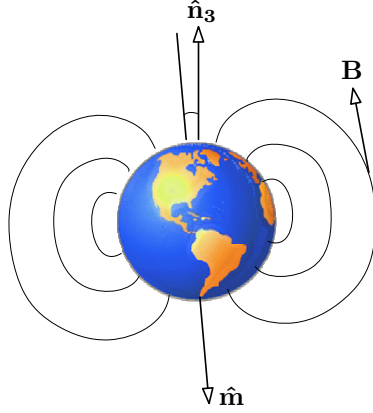

Figure 2: Tilted Dipole Magnetic Field Model

The two remaining unit vectors of the magnetic field frame, $\hat{\mathbf{o}}_1$ and $\hat{\mathbf{o}}_2$, require two reference planes to define them. The first plane contains both $\hat{\mathbf{n}}_1$ and the dipole direction vector, $\hat{\mathbf{m}}$. The second plane is perpendicular to $\hat{\mathbf{o}}_3$. The line of nodes created by the intersection of these two planes defines $\hat{\mathbf{o}}_1$, as depicted in Figure 3. The mathematical definition of $\hat{\mathbf{o}}_1$ is

$$\hat{\mathbf{o}}_1 = \hat{\mathbf{o}}_3 \times (\hat{\mathbf{m}} \times \hat{\mathbf{n}}_1) \tag{3}$$

The vector $\hat{\mathbf{o}}_2$ is defined by $\hat{\mathbf{o}}_2 = \hat{\mathbf{o}}_3 \times \hat{\mathbf{o}}_1$.

The thrust control angle, ψ, gives the direction of the force in the $\hat{\mathbf{o}}_1, \hat{\mathbf{o}}_2$ plane. Solving for the control angle history as a function of time is the main goal of this problem.
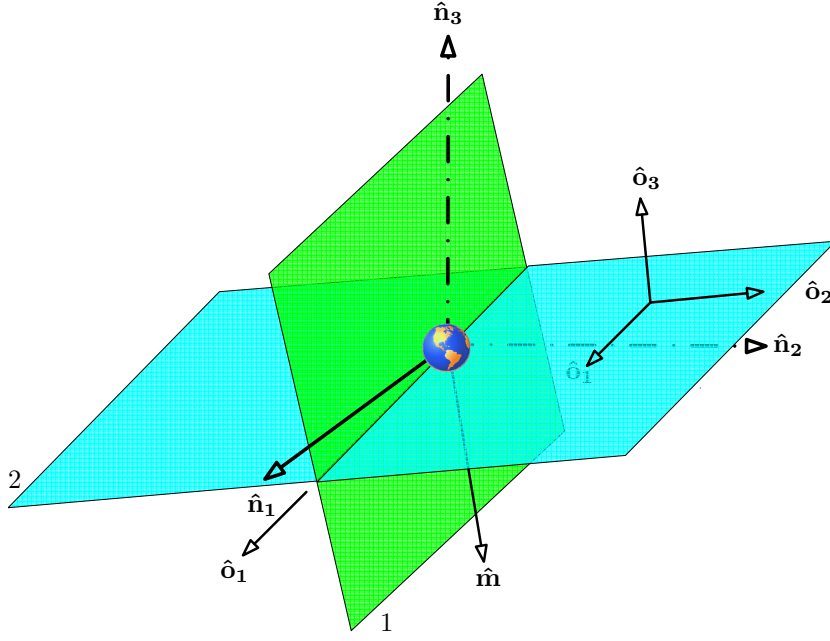
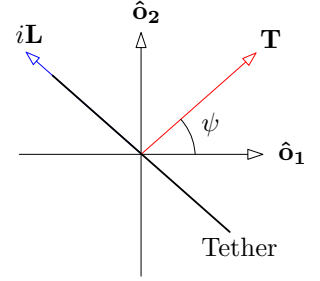Figure 3: Magnetic Field Frame Definition

Figure 4: Control Angle Definition

2.3   Equations of Motion

The derivation of the twelve equations of motion follows the methods given by Thorne and Hall.[9, 10] We assume the EDT and the attracting body are point masses and that the only other external force is the Lorentz force. First, the second-order equations of motion are written as a system of first-order differential equations

$$\dot{x} = v_x \tag{4}$$

$$\dot{y} = v_y \tag{5}$$

$$\dot{z} = v_z \tag{6}$$

$$\dot{v}_x = -\frac{\mu}{r^3}x + \frac{f_x}{m} \tag{7}$$

$$\dot{v}_y = -\frac{\mu}{r^3}y + \frac{f_y}{m} \tag{8}$$

$$\dot{v}_z = -\frac{\mu}{r^3}z + \frac{f_z}{m} \tag{9}$$

where $r = \sqrt{x^2 + y^2 + z^2}$, $f_{()}$ is the scalar component of a perturbation force in the x, y, or z direction, and μ is the gravitational parameter for the attracting body. Here, x, y, and z are components of the EDT position vector with respect to the origin of the ECI frame, N, and v_x, v_y, and v_z are the derivatives of x, y, and z with respect to the inertial frame. To simplify the analysis, the magnetic force vector is represented in F frame coordinates. A coordinate transformation is required to rotate this vector to the inertial frame.

$$\begin{bmatrix} f_x \\ f_y \\ f_z \end{bmatrix}_N = [\mathbf{R}] \begin{bmatrix} f_x \\ f_y \\ f_z \end{bmatrix}_F \tag{10}$$

4

$$\begin{bmatrix} f_x \\ f_y \\ f_z \end{bmatrix}_N = \begin{bmatrix} C_{11} & C_{12} & C_{13} \\ C_{21} & C_{22} & C_{23} \\ C_{31} & C_{32} & C_{33} \end{bmatrix} BiL \begin{bmatrix} \cos\psi \\ \sin\psi \\ 0 \end{bmatrix}_F \tag{11}$$

$$\begin{bmatrix} f_x \\ f_y \\ f_z \end{bmatrix}_N = BiL \begin{bmatrix} C_{11}\cos\psi + C_{12}\sin\psi \\ C_{21}\cos\psi + C_{22}\sin\psi \\ C_{31}\cos\psi + C_{32}\sin\psi \end{bmatrix}_N \tag{12}$$

where C_{ij} is an element in the rotation matrix, $[\mathbf{R}]$. These force components are inserted into Equations 7–9 to form

$$\dot{v}_x = -\frac{\mu}{r^3}x + \frac{BiL}{m}\left(C_{11}\cos\psi + C_{12}\sin\psi\right) \tag{13}$$

$$\dot{v}_y = -\frac{\mu}{r^3}y + \frac{BiL}{m}\left(C_{21}\cos\psi + C_{22}\sin\psi\right) \tag{14}$$

$$\dot{v}_z = -\frac{\mu}{r^3}z + \frac{BiL}{m}\left(C_{31}\cos\psi + C_{32}\sin\psi\right) \tag{15}$$

Equations 4–6 and 13–15 are then used to define the Hamiltonian, $H = \lambda^T \mathbf{d}$, where λ is the Lagrange costate vector defined as $[\lambda_x, \lambda_y, \lambda_z, \lambda_{v_x}, \lambda_{v_y}, \lambda_{v_z}]^T$ and $\mathbf{d}$ is a state vector containing the components of the derivatives of position and velocity. The control law is then obtained by taking the partial derivative of H with respect to ψ and setting it equal to zero

$$\frac{\partial H}{\partial \psi} = \lambda_{vx}\left(-C_{11}\sin\psi + C_{12}\cos\psi\right) + \lambda_{vy}\left(-C_{21}\sin\psi + C_{22}\cos\psi\right) + \lambda_{vz}\left(-C_{31}\sin\psi + C_{32}\cos\psi\right) = 0 \tag{16}$$

which leads to the optimal thrust angle in terms of the costates

$$\psi = \tan^{-1}\left(\frac{-\lambda_{vx}C_{12} - \lambda_{vy}C_{22} - \lambda_{vz}C_{32}}{-\lambda_{vx}C_{11} - \lambda_{vy}C_{21} - \lambda_{vz}C_{31}}\right) \tag{17}$$

This control law is inserted into Equations 13–15 to get the components of velocity in terms of the Lagrange costates:

$$\dot{v}_x = -\frac{\mu}{r^3}x + \beta\left(C_{11} + C_{12}\rho\right) \tag{18}$$

$$\dot{v}_y = -\frac{\mu}{r^3}y + \beta\left(C_{21} + C_{22}\rho\right) \tag{19}$$

$$\dot{v}_z = -\frac{\mu}{r^3}z + \beta\left(C_{31} + C_{32}\rho\right) \tag{20}$$

where β and ρ are defined as

$$\beta = \frac{BiL}{m\sqrt{1 + \left(\frac{-\lambda_{vx}C_{12} - \lambda_{vy}C_{22} - \lambda_{vz}C_{32}}{-\lambda_{vx}C_{11} - \lambda_{vy}C_{21} - \lambda_{vz}C_{31}}\right)^2}} \tag{21}$$

$$\rho = \frac{-\lambda_{vx}C_{12} - \lambda_{vy}C_{22} - \lambda_{vz}C_{32}}{-\lambda_{vx}C_{11} - \lambda_{vy}C_{21} - \lambda_{vz}C_{31}}$$

To complete the analysis, we need six more equations to solve a system with twelve state variables. The remaining equations of motion are

$$\dot{\lambda}_x = -\frac{\partial H}{\partial x} = \frac{\lambda_{vx}\mu}{r^3} - \frac{3\mu x}{r^5}\left(\lambda_{vx}x + \lambda_{vy}y + \lambda_{vz}z\right) \tag{22}$$

$$\dot{\lambda}_y = -\frac{\partial H}{\partial y} = \frac{\lambda_{vy}\mu}{r^3} - \frac{3\mu y}{r^5}\left(\lambda_{vx}x + \lambda_{vy}y + \lambda_{vz}z\right) \tag{23}$$

$$\dot{\lambda}_z = -\frac{\partial H}{\partial z} = \frac{\lambda_{vz}\mu}{r^3} - \frac{3\mu z}{r^5}\left(\lambda_{vx}x + \lambda_{vy}y + \lambda_{vz}z\right) \tag{24}$$

5

$$\dot{\lambda}_{vx} = -\frac{\partial H}{\partial v_x} = -\lambda_x \tag{25}$$

$$\dot{\lambda}_{vy} = -\frac{\partial H}{\partial v_y} = -\lambda_y \tag{26}$$

$$\dot{\lambda}_{vz} = -\frac{\partial H}{\partial v_z} = -\lambda_z \tag{27}$$

We wish to use non-dimensional units in the analysis so that the results are universal and so that the time of flight is simply the change in true anomaly during the maneuver. To complete the transformation, μ is set to unity, and BiL/m is represented by a dimensionless thrust variable, T, defined as

$$T = \frac{BiL/m}{mR_\circ n^2} \tag{28}$$

where n is the dimensional circular orbit velocity at $R_\circ$.

The equations of motion are constructed so that they describe minimum-time motion. In other words, the EDT, whose trajectory is described by the equations of motion, arrives at any given position in the minimum time possible. This formulation makes time of flight a cost function in the optimization problem. The other cost function used is the difference between the position and velocity components of the EDT at $t = t_f$ and the target position and velocity components at $t = t_f$. The other cost function is proportional to how well the EDT matches the target spacecraft's position and velocity. The difference between the position and velocity of the EDT and that of the target spacecraft is called the residual. The EDT meets its target when the residual approaches zero.

2.4   Algorithm

The first step of the algorithm uses a numerical method called simulated annealing (SA). It mimics the physical process of taking a highly unorganized, melted material and reducing the temperature slowly so that the crystalline structure is nearly perfect. Simulated annealing involves lowering the energy state, or performance index, of the system slowly so that the algorithm can find possible minima. As the energy state lowers, the number of possible locations for the global minima within the search space decreases until only one location remains. The exact algorithm for simulated annealing can be found in Refs.[11] and.[12]

Simulated annealing is used to find initial costates and times of flight that produce the smallest residual. The problem with SA is that it has a low convergence rate and low accuracy. The accuracy is refined by using a root-finder, such as `fsolve` in MATLAB. Root-finders have small convergence radii but high convergence rates and high accuracy. Finally, once one solution is found, a family of solutions can be found using Newton's method of continuation.[11]

To obtain full three-dimensional optimal control solutions, comparable two-dimensional solutions must be found first. In the two-dimensional problem, the target orbit is in the earth equatorial plane and $\hat{\mathbf{m}}$ points in the $-\hat{\mathbf{n}}_{\mathbf{3}}$ direction. Having the dipole in the $-\hat{\mathbf{n}}_{\mathbf{3}}$ direction keeps the electromagnetic force in the $\hat{\mathbf{n}}_{\mathbf{1}} - \hat{\mathbf{n}}_{\mathbf{2}}$ plane because $\mathbf{B}$ is always perpendicular to the plane. Also in the two-dimensional case, the N frame and the F frame have the same orientation because of how each frame is defined.

The SA algorithm finds an initial guess for a two-dimensional system, which is then refined to a solution within a specified tolerance. The two-dimensional solution is used as an initial guess for a full tilted dipole problem in three-dimensional space.

3   Results

To gain insight into the EDT optimal control problem, we start with the simple two-dimensional case and compare it to the literature. In the two-dimensional case, the magnetic field model used is a non-tilted dipole, and all orbits are in the equatorial plane. We then use the two-dimensional solutions to develop three-dimensional trajectories.

3.1 Two-Dimensional Optimal Control Problem

Several conclusions can be drawn from studying the two-dimensional problem. As a reference, the following results are compared to the work of Hall and Collazo-Perez.[9] Their work focused on constant thrust, minimum-time optimal phasing maneuvers in two-dimensional space. The authors provided several solutions that were representative of their work and trends that encompassed their results. Two aspects of their work can be directly compared to the two-dimensional EDT optimal control problem. One comparison is obviously the trajectory. The other is the near-invariance of the initial costates when changing the dimensionless thrust and phase angle by an order of magnitude.

3.1.1 Trajectory Analysis

When comparing the optimal trajectory of a constant current EDT with that of a constant thrust spacecraft, intuition suggests that the EDT will catch up to its target faster because thrust increases when the orbit radius decreases, in accordance with (1). A higher thrust should propel the EDT to the target more quickly than a constant thrust model.

Calculations show that the EDT does indeed arrive at its target more quickly. Figures 5 and 6 illustrate a comparison between the trajectories for an EDT and a spacecraft with constant thrust. The red, dotted line is the original orbit and the blue, solid line is the trajectory. In the case depicted, $T_0 = 0.5$ and $\phi = 1.46$ rad, where T_0 is the dimensionless thrust at the original orbit radius. The value for thrust is unusually large for an EDT, but this example is chosen so that differences in their trajectories would be obvious on a plot of the transfer trajectories. The plot shows the EDT arriving at its target about 0.3 TU before the constant thrust spacecraft arrives. Also the shape of the path at mid-flight is more rounded for the constant thrust trajectory than for the EDT trajectory. As stated by Equations 1–2, thrust is proportional to R^{-3}. The increase in thrust give the EDT the ability to fly almost directly at its target, thus creating the flattened shape in its trajectory.
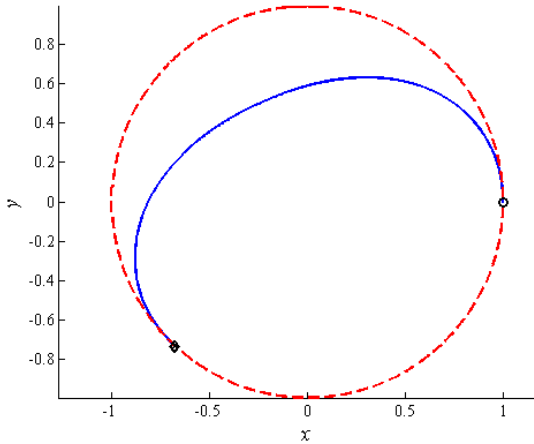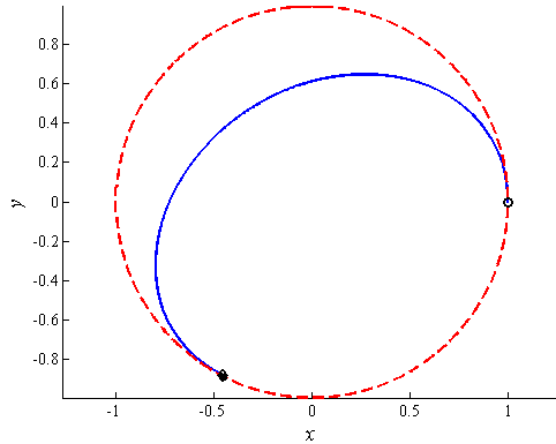

Figure 5: EDT Trajectory   Figure 6: Constant Thrust Trajectory

As stated before, a large phase angle and a large thrust illustrate the EDT's shorter time of flight, but the time of flight for the EDT is shorter than the constant thrust spacecraft for all cases. When comparing initial costates presented in Ref.[9] with the EDT initial costates for several cases, the EDT reaches its target faster in every case. Table 2 illustrates this fact. The difference in time of flight is more pronounced in large phase angle maneuvers. For the case with $\phi = 0.54$, the difference in time of flight is 0.0882 Time Units (TU) while the difference in time of flight is only 0.001525 TU for $\phi = 0.0074$ rad. The small phase angle does not allow the EDT to dip far enough into the orbit to use its advantage over the constant thrust spacecraft.

Figures 7 and 8 show the control angle, ψ, for each spacecraft. For the two-dimensional case, ψ is measured with respect to $\hat{\mathbf{n}}_1$. The shapes are similar with the control angles starting in the third quadrant

Table 2: Lagrange Costate Comparison

		$T_0 = 0.5,$ $\phi = 1.46$	$T_0 = 0.5,$ $\phi = 0.54$	$T_0 = 0.05,$ $\phi = 0.89$	$T_0 = 0.005,$ $\phi = 0.0074$	$T_0 = 0.005,$ $\phi = 0.022$	$T = 0.005$ $\phi = 0.1$
EDT	λ_{y_0}	0.42896	0.099345	0.34992	0.18569	0.43658	0.33357
	$\lambda_{v_{x_0}}$	0.62643	0.65774	0.44331	0.72805	0.69926	0.43892
	$\lambda_{v_{y_0}}$	0.42613	-0.039660	0.98215	0.000697	0.49590	0.99619
	t_f	2.51007	1.95232	5.42443	2.45092	3.78494	6.16831
Constant	λ_{y_0}	0.47313	0.14480	0.34156	0.18627	0.43713	0.33270
Thrust	$\lambda_{v_{x_0}}$	0.63251	0.66574	0.43092	0.72812	0.69905	0.43752
	$\lambda_{v_{y_0}}$	0.49960	0.00012	1.00027	0.001362	0.49755	0.99824
	t_f	2.78398	2.04048	5.58198	2.45245	3.79228	6.18639

to lower the orbit and increase speed. The thrust then rotates 180° at the half way point to raise the orbit to meet with the target. The control angle rotates in this manner for all cases studied.
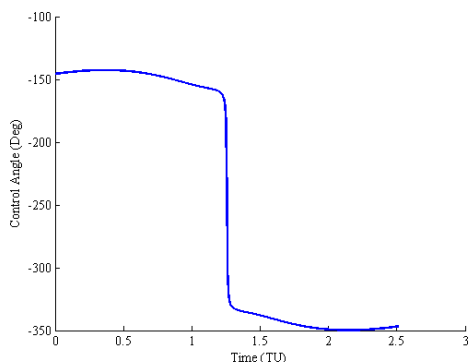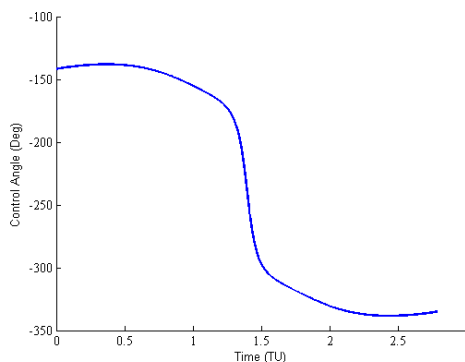

Figure 7: EDT Control Angle

Figure 8: Constant Thrust Control Angle

3.1.2 Near-Invariance of the Initial Lagrange Costates

One important discovery in Ref.[9] is that when T and ϕ are both increased by an order of magnitude, the values of the initial Lagrange costates and the time of flight change by a small amount for moderate and low thrust cases. This near-invariance of the initial costates is important because it allows for the calculation of a whole family of solutions once one solution is found. This trait is also present in the EDT two-dimensional optimal control problem.

Table 3 gives three representative examples that validate the claim of near-invariance for moderate and low thrust cases and shows its limitations. The first example, the case with the lowest thrust value in the group, has the least amount of variance as T and ϕ are increased by an order of magnitude. The costates and the time of flight are constant to three decimal places. The second example shows an invariance between the two costate sets with a precision of two significant digits. The last example compares a high thrust, $T = 0.5$, with a thrust one order of magnitude smaller. This comparison shows the most variation of all the three cases. Further exploration shows large variations in the initial costates when large values of T and ϕ are decreased by an order of magnitude. The large variations in the costates are caused by the different ranges of thrust magnitudes experienced during the maneuver. There is a larger difference in the thrust range experienced during the maneuver in Example 3 than there is during the maneuver in Example 1. A larger thrust range causes a greater variance between costate sets.

Table 3: Demonstration of Near-Invariance of the Initial Costates

	T	ϕ	λ_{y_0}	$\lambda_{v_{x0}}$	$\lambda_{v_{y0}}$	t_f
1	0.0005	0.00074	0.18527	0.72864	-0.0003115	2.45355
	0.005	0.0074	0.18569	0.72805	0.000697	2.45092
2	0.009197	0.001	-2.52311	0.34754	-0.85886	0.66334
	0.09197	0.01	-2.48727	0.34688	-0.84637	0.66314
3	0.05	0.146	0.38861	0.71940	0.32728	3.18374
	0.5	1.46	0.42896	0.62643	0.42613	2.51007

3.2 Three-Dimensional Optimal Control Problem

Now that two-dimensional solutions for the EDT optimal control problem have been established, these solutions can be used as initial guesses to full three-dimensional solutions using the tilted-dipole model. These initial guesses prove to only be useful to find zero inclination phasing maneuvers. Also not all two-dimensional solutions can be used as initial guesses. Solutions with phase angles over 0.01 radians or thrusts over 0.01 do not converge when using `fsolve`. When a three-dimensional, zero inclination angle solution is found, the reason behind the small convergence radius becomes clear. The F frame rotates greatly with time relative to the inertial frame due to the changes in $\mathbf{B}$, and by extension the $\hat{\mathbf{o}}_3$ vector. Because the thrust vector is constrained to $\hat{\mathbf{o}}_1 - \hat{\mathbf{o}}_2$ plane, which can rotate rapidly with the passage of time, the algorithm has difficulty converging to an solution. Once a solution is found, one must consider the dynamics of the solution. Because the thrust is always perpendicular to the magnetic field, the EDT generates the most thrust when it is in the $\hat{\mathbf{o}}_1 - \hat{\mathbf{o}}_2$ plane. For this optimal control to work, the tether must not only rotate about $\hat{\mathbf{o}}_3$, but it must also rotate as the F frame rotates.

3.3 Case Study: Changing Orbit Plane Inclination Angle

In this section, we analyze the changes of the initial costates and the time of flight as the orbit inclination increases from 0°–7.5°. The constant variables in this case study are the phase angle and the product of the tether current and tether length, iL. The values of these variables are 0.002 radians and 300 A-m, respectively. The product of the current and tether length are non-dimensionalized using (28).

The task of finding phasing maneuver solutions for increasing inclination angles is a difficult one because of the trajectory's high sensitivity to the initial guess. Changing an initial guess by 1% can cause the tether to be off target by a distance on the order of 100 km. The high sensitivity is due to the changing magnetic environment caused by the tilted magnetic dipole.

The sensitive nature to the initial guess is not reflected in all initial conditions. The appearance of the plots for each initial condition as a function of the inclination angle can be divided into two groups. Figure 3.3 represents Group 1, which includes λ_y and λ_{v_x}, and Figure 3.3 represents Group 2, which includes λ_z, λ_{v_y}, λ_{v_z} costates and t_f. The slopes of the data in Group 1 change rapidly as i increases, making the task of predicting new solutions using continuation difficult. On the other hand, the new solutions for the initial conditions in Group 2 are easy to predict because the slope changes gradually. The data in Group 2 can be curve-fitted using a linear regression technique and extruded to make a new prediction for a higher inclination angle.

3.3.1 Control Angle Analysis

Two distinct control angle patterns appear for the inclination angle range analyzed in this paper. For inclination angles between 0 and 2 degrees, the control angle plot looks like Figure 11. The overall trend is that the angle continuously decreases over time. A similar trend is seen for the half-orbit 2D solutions as presented in Section 3.1.1, which makes sense because having inclination angles below 2° creates a similar magnetic environment to that in the 2D problem.

For inclination angles between 3 and 7.5 degrees, the control angle plot looks like Figure 12. Here ψ is in the third quadrant for almost half the manuever in order get inside the target orbit to catch up. The control angle then spins around with an increasing ψ to the first quadrant to slow down before finishing the maneuver in the fourth quadrant. If the two control angle plots are compared, the figures show that the
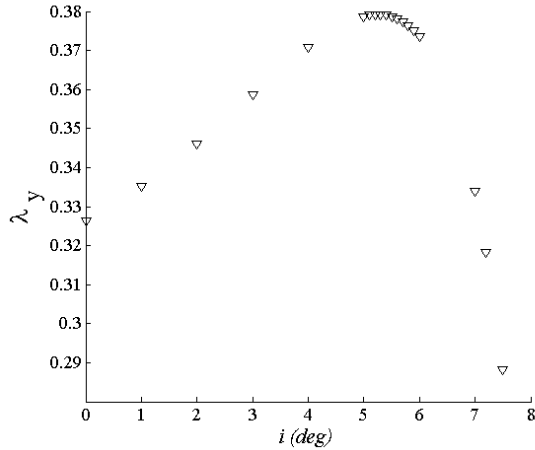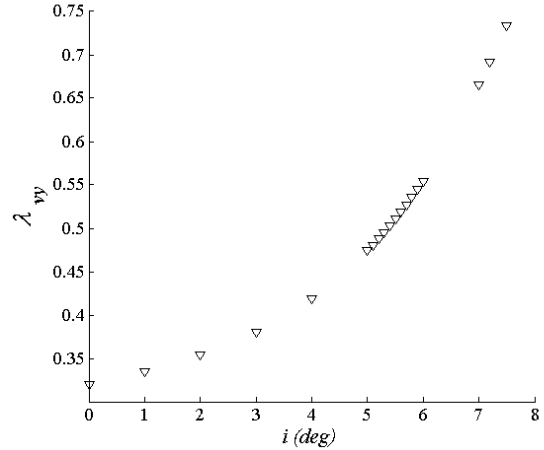
Figure 9: Variations of Group 1 with Increasing i

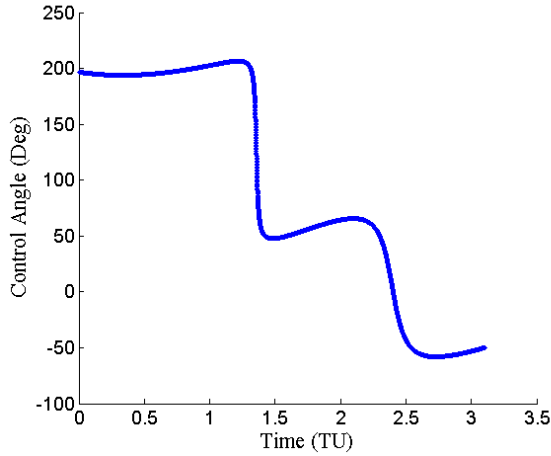
Figure 10: Variations of Group 2 with Increasing i

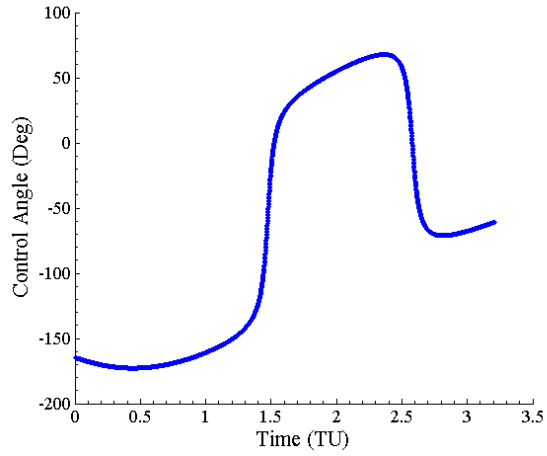Figure 11: Control Angle for $i = 1°$

Figure 12: Control Angle for $i = 5°$

control angles beyond 1.8 TU are almost identical. The only difference in ψ is the direction that the EDT spins after the initial portion of the maneuver. This change in spin direction is also apparent in Ref.[9] when a parameter, in that case an initial costate, is changed by a small amount.

4   Conclusion

Solutions to the minimum-time, constant-current orbit phasing maneuver for an electrodynamic tether have been found for a wide range of two-dimensional cases as well as limited three-dimensional cases. The two-dimensional results are compared with existing data from the literature to provide insight into the characteristics of the solutions. In all cases, the EDT reaches its target faster than a constant thrust spacecraft because the Lorentz force acting on the tether increases as orbit radius decreases. Also sets of initial Lagrange costates, whose parameters T and ϕ each vary by an order of magnitude, are shown to be near-invariant for moderate to low values of thrust and phase angle. These two-dimensional solutions are used as initial conditions to solve for three-dimensional solutions which include a tilted-dipole magnetic field model. These initial conditions are only useful for zero inclination orbits. The most inclined orbit phasing maneuver solved at the time of publication is at $5°$. The reason for the difficulty in converging to a more inclined solution is due to the rotation of the F frame.

10

Further research is needed to fully develop three-dimensional solutions for inclination angles over 7.5° and for phase angles and current values different than those analyzed in this paper. The behavior of the F frame becomes more erratic as inclination angle increases and must be taken into account when finding additional solutions. After more solutions have been found, the same solution algorithm presented can be used to find optimal trajectories for other combinations of ϕ and iL and for other simple maneuvers such as inclination angle change and orbit radius change. These basic maneuvers must be solved in order for electrodynamic tethers to become practical.

References

[1] Williams, Paul. "Optimal Orbit Transfer with Electrodynamic Tethers." *Journal of Guidance, Control, and Dynamics*, Vol. 28, No. 2, 2005, pp. 369-372.

[2] Pearson, Jerome, Levin, Eugene, Carroll, Joseph, Oldson, John. "Orbital Maneuvering with Spinning Electrodynamic Tethers." 2nd International Energy Conversion Engineering Conference, AIAA 2004-5715, Providence, RI, 2004.

[3] Tragesser, Steven G and San, Hakan. "Orbital Maneuvering with Electrodynamic Tethers." *Journal of Guidance, Control, and Dynamics*, Vol. 26, No. 5, 2003, pp. 805-810.

[4] Mankala, Kalyan K. and Agrawal, Sunil K. "Equilibrium-to-Equilibrium Maneuvers of Rigid Electrodynamic Tethers." *Journal of Guidance, Control, and Dynamics*, Vol. 28, No. 3, 2005, pp. 541-545.

[5] Someniz, L., Iess, L., and Pelaez, J. "Linear Stability Analysis of Electrodynamic Tethers." *Journal of Guidance, Control, and Dynamics*, Vol. 28, No. 5, 2005, pp. 843-849.

[6] Beletsky, V. V. and Levin, E. M., *Dynamics Of Space Tether Systems (Advances in the Astronautical Sciences)*. American Astronautical Society, August 1993.

[7] Plugged Into Space. `http://science.nasa.gov/newhome/headlines/ast15oct98\_1.htm`. NASA, 15 October, 1998.

[8] Makovec, Kristin L. *A Nonlinear Magnetic Controller for Three-Axis Stability of Nanosatellites*. Master's Thesis, Virginia Tech, Blacksburg, VA, 2001.

[9] Hall, Christopher D. and Collazo-Perez, Victor. "Minimum-Time Orbital Phasing Maneuvers." *Journal of Guidance, Control, and Dynamics*, Vol. 26, No. 6, 2003, pp. 934-941.

[10] Thorne, James D. and Hall, Christopher D. "Approximate Initial Lagrange Costates for Continuous-Thrust Spacecraft." *Journal of Guidance, Control, and Dynamics*, Vol. 19, No. 2, 1996, pp. 283-288.

[11] Kim, Mischa. *Continuous Low-Thrust Trajectory Optimization: Techniques and Applications*. Ph.D. Dissertation, Virginia Tech, Blacksburg, VA, 2005.

[12] Aarts, E. and Korst, J. *Simulated Annealing and Boltzmann Machines: a Stochastic Approach to Combinatorial Optimization and Neural Computing*. John Wiley & Sons, Inc., New York, NY, 1989.